Geophys. J. Int. (2004) **157,** 1105–1118 doi: 10.1111/j.1365-246X.2004.02309.x

Simulated geomagnetic reversals and preferred virtual geomagnetic pole paths

C. Kutzner and U. R. Christensen

Max-Planck-Institut für Aeronomie, Katlenburg-Lindau, Germany. E-mail: christensen@linmpi.mpg.de

Accepted 2004 March 25. Received 2004 March 25; in original form 2003 November 3

SUMMARY

The question of whether virtual geomagnetic poles (VGPs) recorded during reversals and excursions show a longitudinal preference is a controversial one amongst palaeomagnetists. One possible mechanism for such VGP clustering is the heterogeneity of heat flux at the core–mantle boundary (CMB). We use 3-D convection-driven numerical dynamo models with imposed non-uniform CMB heat flow that show stochastic reversals of the dipole field. We calculate transitional VGPs for a large number of token sites at the Earth's surface. In a model with a simple heat flux variation given by a Y_{22} harmonic, the VGP density maps for individual reversals differ substantially from each other, but the VGPs have a tendency to fall around a longitude of high heat flow. The mean VGP density for many reversals and excursions shows a statistically significant correlation with the heat flow. In a model with an imposed heat flux pattern derived from seismic tomography we find maxima of the mean VGP density at American and East Asian longitudes, roughly consistent with the VGP paths seen in several palaeomagnetic studies. We find that low-latitude regions of high heat flow are centres of magnetic activity where intense magnetic flux bundles are generated. They contribute to the equatorial dipole component and bias its orientation in longitude. During reversals the equatorial dipole part is not necessarily dominant at the Earth's surface, but is strong enough to explain the longitudinal preference of VGPs as seen from different sites.

Key words: core–mantle coupling, geodynamo model, palaeomagnetism, reversals.

1 INTRODUCTION

Although it has been known since the beginning of the 20th century that the Earth's magnetic field undergoes polarity changes (Brunhes 1906), the first recording of field directions during a transition was reported much later (van Zijl *et al.* 1962). Transitional magnetic field data are needed to understand the nature of geomagnetic reversals, which involves questions of dipole or multipole dominance during a polarity transition or a possible longitudinal bias of the equatorial dipole or other magnetic field components.

The local field directions that can be extracted from rock samples are usually expressed in the form of virtual geomagnetic pole (VGP) positions. For this purpose one assumes that the surface field is that of a geocentric dipole. In this case each pair of declination and inclination (D, I) data unambiguously corresponds to a VGP position. In addition, directional data for any site would give the same VGP position, that of the true geomagnetic pole (TGP), i.e. the south pole of the dipole field alone. Non-dipole contributions to the surface field will result in different VGPs depending on the site where the (D, I) data are taken. The less the dipole hypothesis is valid, the more the VGPs will scatter.

Thus the distribution of the transitional VGPs recorded at different sites gives valuable information about the field structure during that transition. If all the VGPs for a given reversal more or less follow the same path regardless of the site location this indicates a predominantly dipolar transitional field, which was the conclusion of some early publications (Creer & Ispir 1970; Steinhauser & Vincenz 1973). However, Hillhouse & Cox (1976) found that the VGP path for the Matuyama–Brunhes reversal (780 000 BP) obtained from their Californian site substantially differed from that obtained from a site in Japan (Niitsuma 1971). This was taken as evidence for a complex field structure with significant non-dipole contributions to the magnetic field.

More recently, palaeomagnetic studies of reversals and excursions indicated a concentration of VGPs along American and East Asian longitudes. This was not only found for transitions of the last 11 Myr (Tric *et al.* 1991; Laj *et al.* 1991) but also for VGPs that were obtained for the Matuyama–Brunhes reversal alone (Clement 1991; Clement & Kent 1991; Hoffman 2000). It was noted that the areas of high VGP density correlate with regions of high seismic velocity in the lower mantle (Dziewonski & Woodhouse 1987; Laj *et al.* 1991), and that the VGP paths lie close to the longitudes where magnetic flux concentrations at the core–mantle boundary (CMB) are found in the historic field (Jackson *et al.* 2000).

The inferred longitudinal preference of VGP paths has been criticized as a possible artefact. Valet *et al.* (1992) claim that far more

data are required for statistical interpretations of VGP distributions. Langereis *et al.* (1992) and Barton & McFadden (1996) argue that the fidelity of sedimentary data may not be high enough to reliably record and conserve the fast directional changes that occur during field transitions. A study based on volcanic data alone, covering reversals and excursions of the last 16 Myr, showed a random distribution of the VGPs (Prévot & Camps 1993), suggesting that the average transitional field is axisymmetric. On the other hand, in an extensive study of volcanic data from the last 20 Myr, Love (1998) found preferred VGP longitudes that are roughly consistent with those from sedimentary data. Love (2000) used various statistical tests to show that the preference for American and Asian longitudes is robust.

To date, the question of whether transitional VGPs actually follow preferred longitudes or if the clustering is due to peculiarities of the data accumulation process is still open. Here we use a numerical dynamo model to test a possible physical mechanism for VGP clustering.

One reason why the dipole prefers reversing along the Pacific rim was suggested by Runcorn (1992). As the secular variation is low in the Pacific hemisphere, Runcorn proposed that there the geomagnetic field is shielded by a layer of high conductivity at the bottom of the mantle. When in his simple model the dipole begins to reverse along an arbitrary meridian, in this high-conductivity region electric currents are induced. They produce a torque that rotates the core relative to the mantle until the reversing dipole path lies on the rim of the hemispherical region of high conductivity. In a more detailed analysis Brito *et al.* (1999) concluded that this mechanism is unlikely to lead to longitudinal confinement of VGPs.

The finding that the preferred regions of transitional VGPs coincide with areas of high seismic velocity in the lowermost mantle suggests that thermal differences at the CMB could cause the observed clustering. Although the interpretation of seismic velocity heterogeneity in the lower mantle in terms of thermal anomalies alone may be too simple, the correlation of fast velocities near the CMB with subduction zones suggests that these regions are in fact relatively cold. The potential importance of the thermal state of the lower mantle for core fluid motion was originally pointed out by Hide (1967). Because of the large differences in timescales and temperature anomalies characteristic of convection in the core and mantle, respectively, the CMB is nearly isothermal from the perspective of mantle flow. Temperature heterogeneities in the lowermost mantle imply lateral variations of the heat flux imposed on the convecting core at the CMB. The pattern of heat flux is quasi-static from the perspective of core flow. These variations significantly influence the core flow (Bloxham & Gubbins 1987) and break the axial symmetry so that some reversal paths might become more probable than others. The fact that the mean reversal frequency changes on the timescale of mantle convection (10–100 Myr) suggests that the mantle exerts some control on the geodynamo.

Bloxham (2000) showed that a dynamo model with an imposed CMB heat flux variation of degree 2 and order 0 yields a stronger contribution of the octupole to the magnetic field than a model with homogeneous heat flow. Bloxham (2002) and Olson & Christensen (2002) examined time-averaged properties of dynamos with heterogeneous boundary heat flux. The heat flux heterogeneity drives a weak mean flow at the top of the core. The time-averaged CMB magnetic field shows concentrations above downwellings in the time-averaged flow field. Christensen & Olson (2003) studied also the amplitude and pattern of secular variation in such models, finding regional differences in the standard deviation of VGPs from the mean. However, no reversals were observed in these dynamo calculations.

Glatzmaier *et al.* (1999) imposed a non-uniform heat flux pattern on their reversing dynamo model and found the frequency of the reversals to be strongly dependent on the heat flux pattern. Unfortunately the number of reversals was too low for a statistical evaluation. Coe *et al.* (2000) analysed in detail four magnetic field reversals from these models, two of them from a case with non-homogeneous CMB heat flux. They calculated VGPs for a large number of sites distributed over the Earth and found a crude correlation between the density of transitional VGPs and the pattern of CMB heat flux. However, the results for the two reversals differ substantially from each other. They attributed the clustering of VGPs, as seen from different sites, to the equatorial dipole contribution even though it is weaker than the non-dipole field. They concluded that the results appear to support the hypothesis of VGP clustering but that more reversals needed to be analysed to test if the correlation with heat flow is robust.

In this work we extend previous dynamo modelling studies with different imposed CMB heat flux patterns (Olson & Christensen 2002; Christensen & Olson 2003) to the regime where the magnetic dipole reverses stochastically. As shown by Kutzner & Christensen (2002), this requires that the Rayleigh number is increased beyond a certain threshold value (driving of the flow is strong enough). We calculate time-averaged VGP distributions as well as VGP density maps for individual reversals. We run our models for a sufficiently long time to observe typically 10 reversals and a similar number of excursions. This provides the basis for a statistically robust analysis of longitudinal bias in the distribution of intermediate VGP positions.

2 THE NUMERICAL MODEL

The dynamo simulations are carried out with a modified version of the numerical code originally developed by Glatzmaier (1984); for a description see also Olson *et al.* (1999) and Christensen *et al.* (1999). We consider a spherical shell with an inner radius r_i that is 0.35 times the outer radius r_o. Between the rigid corotating boundaries is an electrically conducting Boussinesq fluid. The inner core and the mantle are assumed to be electrically insulating. The effect of the finite conductivity of the inner core has shown to be negligible in the investigated parameter range (Wicht 2002). We solve the following set of equations, described in Kutzner & Christensen (2002): (i) the Navier–Stokes equation with full inertia, Coriolis, pressure gradient, viscous, buoyancy and Lorentz forces, (ii) the induction equation for the magnetic field, (iii) an equation for the transport of the codensity X, which combines thermal and compositional buoyancy.

The main driving mechanism for convection in our model is compositional, based on the assumption that in the Earth's core buoyancy is primarily created through the release of a light element at the inner core boundary (ICB) as the inner core freezes. If we denote C as the deviation of the concentration of the light element within the core fluid from its mean C_0, then the following transport equation holds:

$$\frac{\partial C}{\partial t} + \mathbf{u} \cdot \nabla C = \kappa_C \nabla^2 C - \gamma_C \tag{1}$$

with κ_C being the chemical diffusivity. The effective sink term γ_C enters the equation because we assume that the mean concentration increases linearly with time, $C_0(t) = C_0(0) + \gamma_C t$. The equation for the transport of heat is:

$$\frac{\partial T}{\partial t} + \mathbf{u} \cdot \nabla T = \kappa_T \nabla^2 T + \gamma_T, \tag{2}$$

where T is the deviation from an adiabatic reference state $T_0(r, t)$, which is likewise time dependent because of core cooling. Apart from possible radiogenic heat sources, the rate of core cooling and the conductive heat flux along the adiabatic gradient contribute to γ_T. While γ_T will in general be a function of radius, for simplicity we assume the adiabatic gradient to be proportional to $-r^2$, which makes γ_T independent of r. Depending on the cooling rate and on the amount of radiogenic heat sources, γ_T can be positive or negative.

The two equations (1) and (2) can be merged into a single one if one assumes the thermal and chemical diffusivities to be the same, $\kappa_T = \kappa_C = \kappa$. While the molecular values of κ_C and κ_T differ strongly, the effective diffusivities due to turbulent mixing would be more equal. Multiplying eq. (2) with the coefficient of thermal expansion α and adding it to eq. (1) yields an equation for the transport of the so-called 'codensity' X (Braginsky & Roberts 1995; Sarson *et al.* 1997), which we define as $X = (\Delta\rho_C/\rho_0)\, C + \alpha T$; with $\Delta\rho_C$ the chemical density contrast and ρ_0 the reference density.

$$\frac{\partial X}{\partial t} + \mathbf{u}\cdot\nabla X = \kappa\nabla^2 X - \gamma. \tag{3}$$

The density ρ in the buoyancy term of the Navier–Stokes equation is then given as $\rho = \rho_0(1 - X)$.

The scales for length, time and magnetic induction are D, D^2/η and $(\rho\eta\Omega\mu_0)^{1/2}$ respectively, with $D = r_o - r_i$ the shell thickness, η the magnetic diffusivity and Ω the rotation rate about the z-axis. X is scaled by $\gamma D^2/\kappa$, which gives a modified Rayleigh number $Ra = \gamma D^3\, g_0/\Omega\,\kappa\nu$ and makes the non-dimensional value of γ in eq. (3) equal to 1. The other non-dimensional input parameters are the Prandtl number $Pr = \nu/\kappa$, the Ekman number $E = \nu/(\Omega D^2)$ and the Roberts number $q = \kappa/\eta$. Here ν is the kinematic viscosity and g_0 the gravity at the outer radius r_o.

At the inner boundary we assume a fixed uniform flux of codensity $f_i = (-\partial X/\partial r)_{r=r_i}$ according to the constant release of light element and associated release of latent heat due to growth of the inner core. We assume that the compositional flux across the CMB is zero and that here only the thermal component contributes to the flux of codensity. Furthermore, we assume that the total codensity flux at the outer boundary $f_o = (-\partial X/\partial r)_{r=r_o}$ has a zero mean value, i.e. in terms of spherical harmonic expansion $f_o(\ell = 0, m = 0) = 0$. In the framework of the Boussinesq approximation, where only deviations from the adiabatic state are considered, this means that the total amount of heat that leaves the core exactly equals the heat conducted along the adiabat. On top of the zero mean we add different heat flux patterns, so that the heat flux is superadiabatic in some regions and subadiabatic in others. Hence the net driving of convection is purely compositional, but thermal buoyancy, being neutral on average, modulates the driving buoyancy forces in particular near the CMB. The value of the flux at the inner boundary is set such that it exactly compensates the internal sinks of X. For our chosen geometry this implies a non-dimensional value of $f_i = 3.9963$.

Here we concentrate on two different patterns of heat flow heterogeneity, described by a simple Y_{22} spherical harmonic and derived from a seismic tomography model of the lower mantle, respectively. For these two cases, the deviations from the mean adiabatic heat flux are shown in Figs 1(g) and (h). The tomographic heat flux pattern is taken from the seismic tomography model by Masters *et al.* (1996) and contains spherical harmonics up to degree and order 4. Seismic velocity heterogeneity in the mantle can arise from differences in composition or temperature. For simplicity we attribute the lateral changes in wave velocity to differences in temperature alone. With this assumption, high seismic velocity above the CMB translates into low temperature, which means high heat flux across the CMB. Accordingly, low seismic velocities correspond to low heat flux. The resulting pattern is a ring structure of enhanced heat flux around the Pacific. The Y_{22} heat flux pattern can be regarded as a crude approximation to the tomographic pattern, because the harmonic of degree and order 2 contributes most to the anomaly in the lowermost mantle. A possible correlation between non-zonal structures in the dynamo-generated magnetic field and the heat flow can be perhaps more easily extracted for this simple pattern, which has also been used in several previous studies (Sarson *et al.* 1997; Glatzmaier *et al.* 1999; Gibbons & Gubbins 2000). In addition, we also studied a few models with a purely zonal heat flow distribution (Figs 1a–d). These models should not show any longitudinal bias in the VGP distribution; however, the heat flow heterogeneity can affect the frequency of reversals (Glatzmaier *et al.* 1999).

The amplitude of the heat flux variation $f_o(\ell, m)$ is set to one of the values 0.0, 0.088, 0.106 or 0.176. In the case of the tomographic model we mean by amplitude that of the dominant Y_{22} mode. The spatial variation of the codensity flux on the outer boundary may appear small compared with the total codensity flux at the ICB of $f_i \approx 4$. However, the same total flux passing through the outer boundary corresponds to $f_o(0, 0) = 0.49$, so that the imposed variations are a significant fraction of the equivalent flux. There are indications for a (parameter-dependent) upper limit for the heat flux variation that the dynamo can tolerate. Olson & Christensen (2002) found that their dynamos failed when the amplitude of the imposed heat flux heterogeneity exceeded a critical value. All models described in this study sustained a magnetic field when $f_o(\ell, m) \leq 0.176$.

The computations are done with 40 radial grid intervals and with a spectral resolution up to a maximum harmonic degree of $\ell_{max} = 85$. The non-dimensional input parameters we use in this study are $E = 3 \times 10^{-4}$, $q = 3$, $Pr = 1$ and different values for the Rayleigh number, usually $Ra = 9000$. With these parameters the kinetic energy spectrum drops by more than a factor of 1000 from the peak to the spectral cut-off. However, the magnetic energy spectra fall off more slowly with harmonic degree ℓ, so that in some cases the difference between the peak and the cut-off is only about 30. Still, due to earlier resolution tests (Christensen *et al.* 1999; Kutzner & Christensen 2002) we are confident that the long- and intermediate-wavelength structures (up to a harmonic degree of $\ell \approx 40$) are well resolved. Because of the geometrical attenuation when continuing the field to the Earth's surface, only the very first harmonics are important for the calculation of the VGPs.

As initial conditions for the models we took the output of previous dynamo runs with similar input parameters, so that in most cases only the boundary condition at r_o had to be changed. We excluded the first magnetic diffusion time unit of each run from the analysis, as it can be affected by transient effects.

3 RESULTS

A summary of the simulations is given in Table 1. The magnetic Reynolds number $Rm = u_{rms} D/\eta$ is based upon the rms velocity in the shell. The magnetic energy density in the shell is given by

$$E_{mag} = \frac{1}{2V_s Eq\, Pr}\int_{V_s} \mathbf{B}^2\, dV \tag{4}$$

with V_s being the volume of the fluid shell. We have further listed the contribution of the dipole to the magnetic energy density in the shell, $\overline{E}^{\ell=1}_{mag}$, and to the CMB field strength, $\overline{B}_{dip}$. Overbars indicate that the values have been time averaged. The last column of Table 1 gives the average number of reversals per magnetic diffusion time

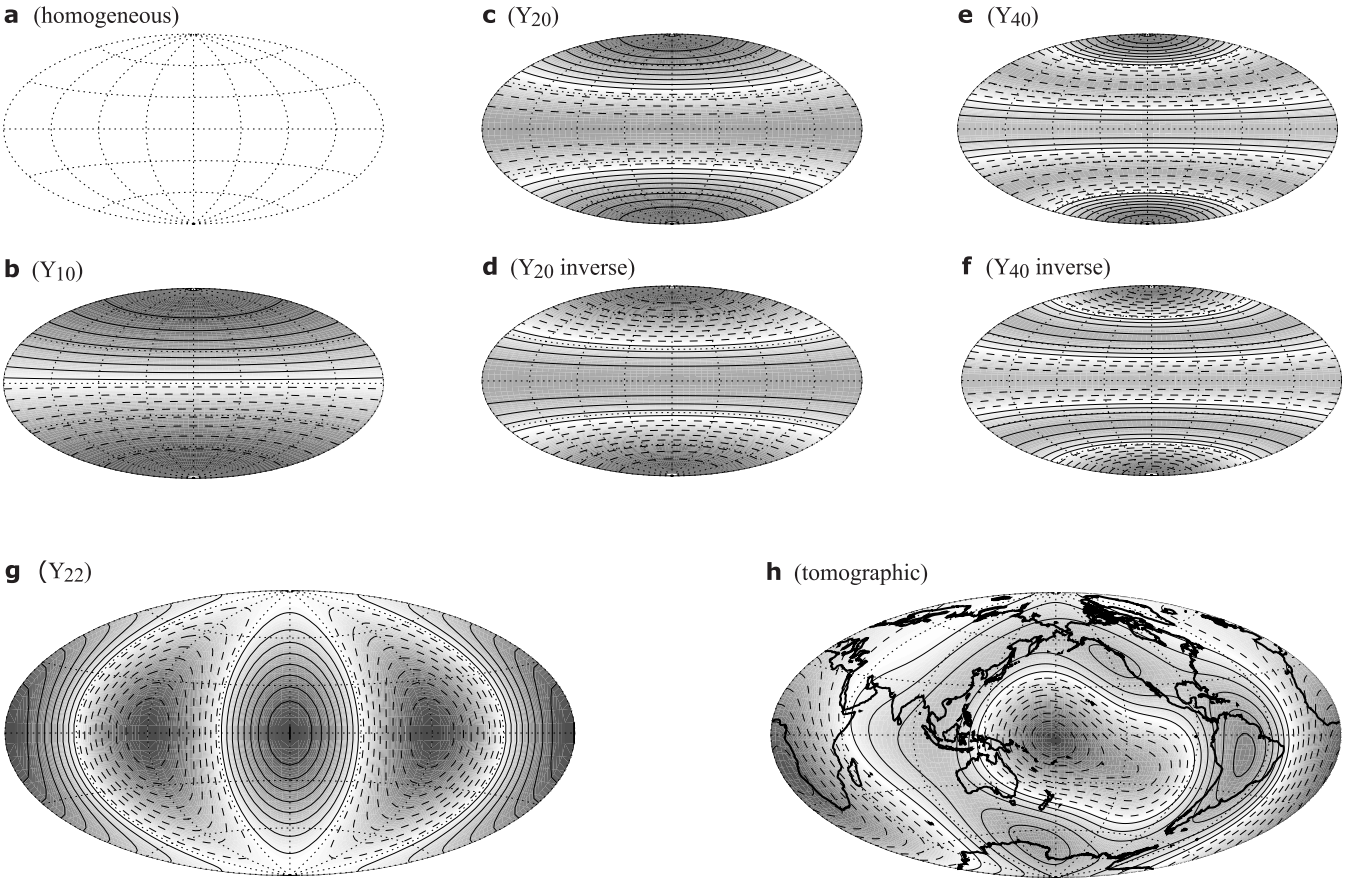

Figure 1. Imposed CMB heat flux patterns. Heat flux is superadiabatic within the solid contours and subadiabatic within the broken contours. Shading indicates the amplitude. Zero longitude is in the centre, except in the tomographic case, which is centred at 180°.

Table 1. Time-averaged properties of the dynamo runs. Input parameters are $E = 3 \times 10^{-4}$, $q = 3$, $Pr = 1$. The Rayleigh number is given in the third column. The last column gives number of reversals per magnetic diffusion time unit. A dash means that no reversals occurred during the simulation.

Heat flux pattern	Ampl. f_o	Ra	$\overline{Rm}$	$\overline{E}_{\rm mag}$	$\overline{E}_{\rm mag}^{\ell=1}$ (per cent)	$\overline{B}_{\rm CMB}$	$\overline{B}_{\rm dip}$	Rev. frequency
Uniform	0.000	9000	511	2960	1.5	0.34	0.053	2
Y_{10}	+0.106	9000	571	2910	3.0	0.24	0.039	1
Y_{20}	+0.106	9000	474	3350	1.9	0.45	0.134	–
Y_{20}	−0.106	9000	566	2110	1.2	0.24	0.028	8
Y_{40}	+0.106	9000	534	2510	1.3	0.31	0.033	6
Y_{40}	−0.106	9000	479	3950	2.0	0.46	0.130	–
Y_{22}	+0.106	9000	520	3200	2.0	0.37	0.064	1
Y_{22}	+0.106	6000	426	2660	2.6	0.36	0.093	0.5
Y_{22}	+0.106	3000	292	2490	4.4	0.43	0.199	–
Y_{22}	+0.176	9000	526	3200	1.9	0.36	0.066	2
Tomographic	0.088	9000	509	2700	1.7	0.31	0.046	2
Tomographic	0.088	6000	428	1550	1.7	0.23	0.035	2
Tomographic	0.176	9000	503	2020	1.1	0.27	0.024	2

unit of the simulation. There is some ambiguity in defining of what constitutes a reversal and we have adopted the following procedure. We smooth the time-series of the tilt of the magnetic dipole by taking a running average with a moving window of 0.15 time units. Then we count each equator crossing as a reversal. The filtering prevents short-term events, that one would characterize as excursions, from being counted as reversals.

With the exception of two cases all of the dynamos undergo reversals of the dipole axis when the Rayleigh number is set to its maximum value $Ra = 9000$. Fig. 2 shows the time-series of a model with an imposed Y_{22} heat flux pattern as an example for the reversal behaviour. Typically the strength of the CMB dipole field is strongly reduced during excursions and reversals (see for example the reversal at $t \approx 0.5$ and the excursion at $t \approx 1.7$) and periods of a strong dipole contribution to the total field are correlated with small inclinations of the dipole axis against the rotation axis (e.g. at $t \approx 3.3$). This is also the case for a number of other simulated reversals (Glatzmaier *et al.* 1999; Coe *et al.* 2000; Kutzner &

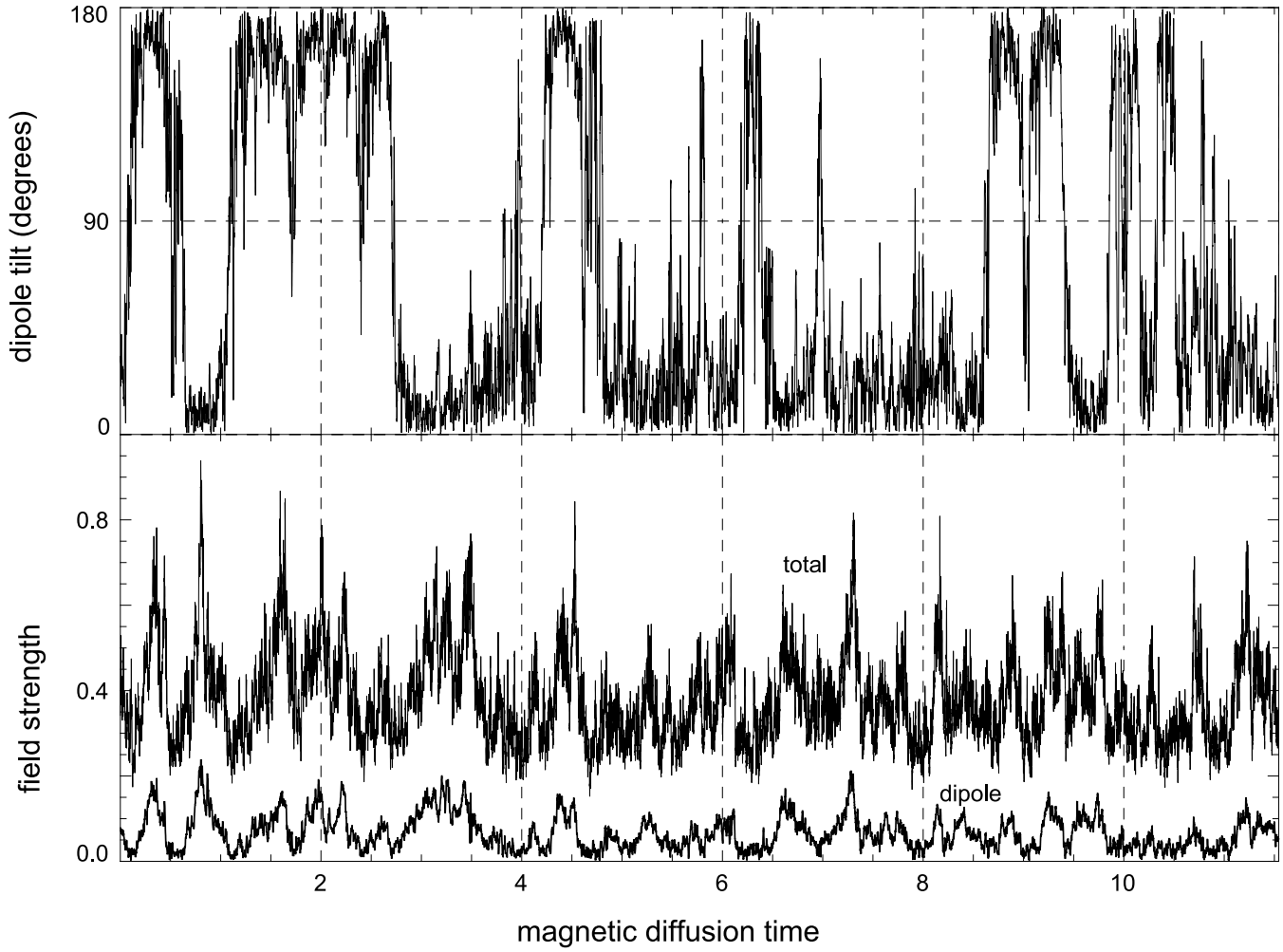

Figure 2. Time-series for the model with imposed Y_{22} heat flux, $f_o = 0.106$, $Ra = 9000$. Upper graph: inclination of the dipole axis. Lower graph: the upper line shows total field strength at the CMB and the lower line the field strength that is due to the dipole field alone. The length of the whole time-series scales to approximately 1.4 Myr.

Christensen 2002) and has been inferred for the geomagnetic field as well (Merrill & McFadden 1999).

If one assumes an electrical conductivity of $\sigma = 6 \times 10^5$ S m^{-1} (Secco & Schloessin 1989) and a density of 10^4 kg m^{-3} in the core, then one magnetic diffusion time unit scales to approximately 122 000 yr for the Earth, and a non-dimensional CMB dipole field of 0.1 corresponds to a dipole moment of approximately 3.3×10^{22} A m^2. The mean dipole moment of the model from Fig. 2 translates into 2.1×10^{22} A m^2, which is about 30–50 per cent of the estimated palaeomagnetic average (Dormy *et al.* 2000; Selkin & Tauxe 2000). The model magnetic field undergoes 14 reversals in approximately 1.4 Myr. The deviation of the dipole axis from the rotation axis frequently becomes large. The distribution of tilt angles as function of latitude peaks at 14° from the poles.

Fig. 3 shows the surface energy spectrum of this model averaged over eight magnetic diffusion times. The instantaneous spectrum is calculated from the Gauss coefficients g_ℓ^m and h_ℓ^m by (Langel & Estes 1982):

$$W(\ell) = (\ell + 1) \sum_{m=0}^{\ell} \left[\left(g_\ell^m\right)^2 + \left(h_\ell^m\right)^2 \right]. \quad (5)$$

In comparison with the instantaneous spectrum of the present Earth the time-averaged model spectrum is displaced to lower values. This

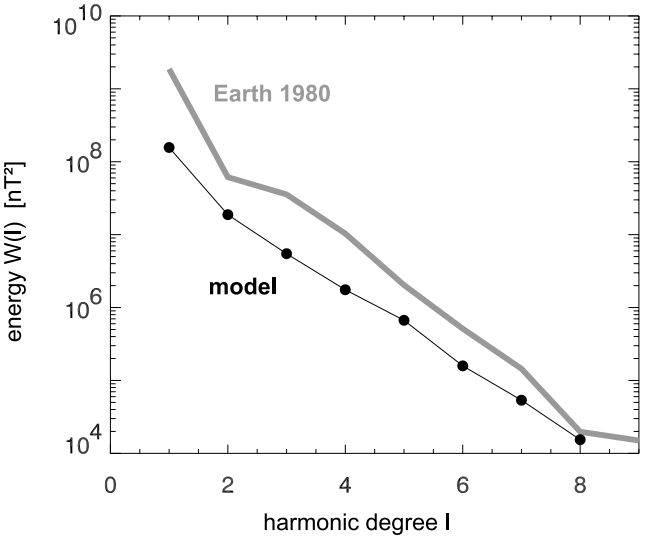

Figure 3. Black line and dots: time-averaged surface energy spectrum of the model with imposed Y_{22} heat flux, $f_o = 0.106$, $Ra = 9000$ (see Fig. 2 for time-series). For comparison the grey line shows the spectrum of the Earth's magnetic field for the year 1980.

is of no consequence for the calculation of VGP positions which depend only on angular data. The general slopes of $W(\ell)$ agree well. Although the dipole contribution typically becomes much smaller during excursions and reversals, the average surface field of the model is dipole-dominated.

In comparison with the Earth's field the magnetic field of this and several other of our dynamo models is slightly weaker and slightly less dipole-dominated on time averaging. Reversals are more frequent, which allows a robust determination of the statistical distribution of transitional VGPs without requiring prohibitively long run times of the models. We would not expect that these differences from the Earth's field have a major influence on the VGP paths.

3.1 Reversal frequency

As demonstrated before by Glatzmaier *et al.* (1999) (in the following G99), the CMB heat flux pattern strongly affects the reversal frequency. At $Ra = 9000$ and an amplitude of flux variation of $f_o = 0.106$ the models $+Y_{20}$ and $-Y_{40}$ (Figs 1c and f) stay in one polarity during the whole simulation, whereas all the other models undergo reversals. The sign in front of the harmonic indicates the sign of the coefficient for the CMB heat flow anomaly, which in case of these two harmonics implies a negative anomaly in the equatorial belt. The time-series of model Y_{22} in Fig. 2 shows an example of the reversal behaviour that is also typical for uniform and tomographic heat flux and in the cases $+Y_{10}$ and Y_{22} (Figs 1b and h). The reversal frequency in the cases $-Y_{20}$ and $+Y_{40}$ (Figs 1d and e) is higher compared with the other cases.

Our results basically agree with those of the G99 study, but with the notable exception of the models $-Y_{40}$ and $+Y_{40}$. Our model $+Y_{40}$ has one of the highest reversal frequencies whereas this heat flux pattern led to a non-reversing dynamo in the G99 study. Our model $-Y_{40}$ exhibits a stable, dipole-dominated field whereas the initial magnetic field of the corresponding model in G99 decays away so that there is no self-sustained dynamo action. G99 argue that the small number of reversals for the heat flux patterns $+Y_{20}$ (one reversal) and $+Y_{40}$ (no reversal) is due to the high heat flux in polar regions which reinforces the polar upwellings. These are surrounded by a thermal wind (Glatzmaier & Roberts 1997) stabilizing the axial dipole.

In contrast, the reversal frequency of our dynamos seems to depend on the sign of the heat flux anomaly in the equatorial region. If the equatorial heat flux is above average as in the cases $-Y_{20}$ and $+Y_{40}$ the reversal frequency is higher compared with the homogeneous case. The models $+Y_{20}$ and $-Y_{40}$ with lower than average equatorial heat flux do not change polarity. The magnetic Reynolds number, as a measure for the average flow velocity, is slightly lower ($Rm \approx 475$) in models $+Y_{20}$ and $-Y_{40}$ compared with the uniform heat flux case with $Rm = 511$. In models $-Y_{20}$ and $+Y_{40}$ with enhanced equatorial heat flow convection is slightly more vigorous ($Rm \approx 550$). A high equatorial heat flux enhances columnar convection outside the inner core tangent cylinder, which makes the main contribution to the overall energy of the flow and which is probably more essential for the dynamo mechanism in our models than convection inside the tangent cylinder (Olson *et al.* 1999). Previously we have shown that in models with uniform boundary conditions the reversal frequency increases with the vigour of convection, controlled in that case by the Rayleigh number (Kutzner & Christensen 2002). Here the flow velocity is affected by different distributions of the heat flow on the outer boundary.

In our models, a possible stabilizing effect of enhanced polar upwelling does not seem to play a significant role. The mechanism by which the overall magnetic field is generated may differ between G99 and our models. While in G99 a strong axisymmetric toroidal field is mainly found inside the tangent cylinder, our dynamos exhibit a strong toroidal field outside the tangent cylinder region as well.

3.2 VGP distribution

For the calculation of the VGPs we continue the CMB field upwards to the surface of the Earth. For a given site and given time the VGP is determined from the declination and inclination of the field at that location. Fig. 4 shows the trajectory of the VGP recordings for an equatorial site for the Y_{22} case from Fig. 2. Each VGP recording is plotted with a dot and consecutive recordings are connected with a line. VGPs are approximately 50 yr apart. Already visual inspection suggests a clustering of VGPs in areas of high CMB heat flux below the site and at the edges of the projection.

In the following analysis we use a large number of sites, distributed randomly over the globe, and consider only VGPs that are more than 30° away from either rotation pole. These VGPs are mainly recorded during reversals and excursions of the dipole field, but they also arise from strong local secular variation at a given site. We refer to them as transitional VGPs.

To determine the mean (site-independent) VGP distribution we calculate the VGPs not only for a single site but for 200 sites (for long-term time-averaged VGP distributions) or for 2000 sites (for individual reversals) that are distributed randomly over the globe.

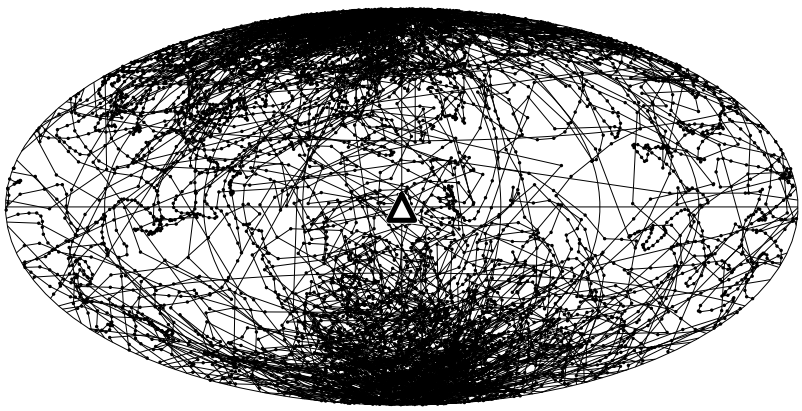

Figure 4. VGP path that would be recorded by a site at the centre of the map (pyramid at latitude $\theta = 0°$, longitude $\phi = 0°$) during the first 4.3 time units of the model from Fig. 2. Maxima of CMB heat flux are located below the site at $\phi = 0°$ and at $\phi = 180°$.

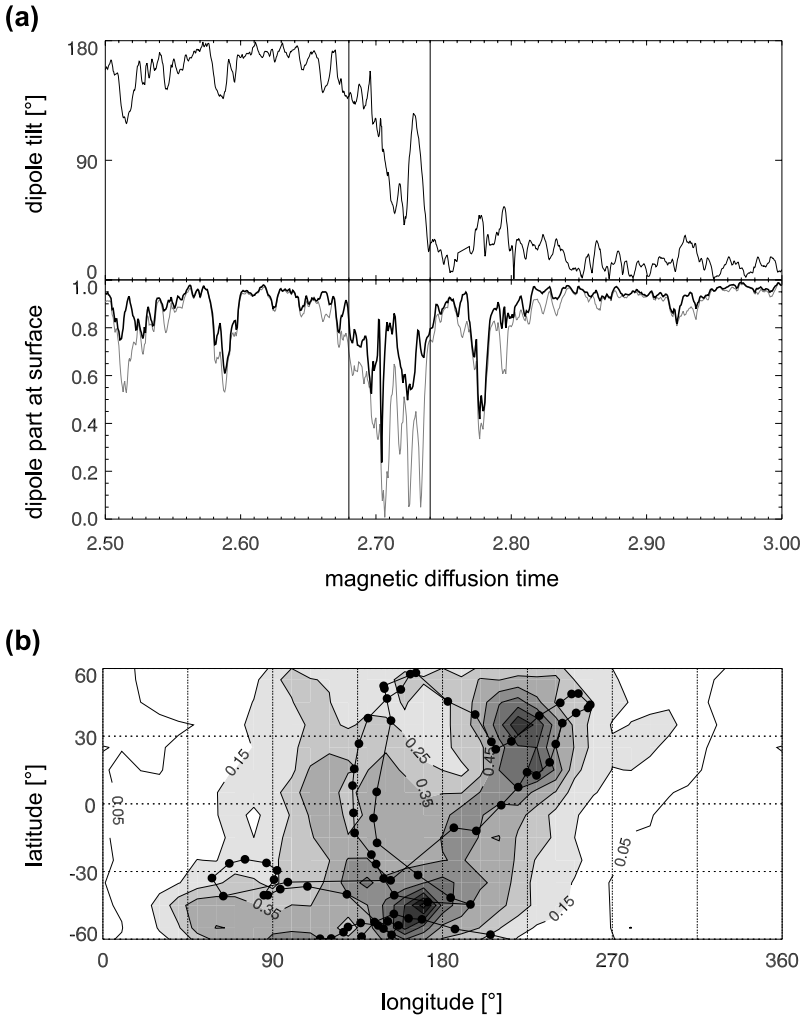

Figure 5. Fourth reversal of the Y_{22} case from Fig. 2. (a) Top: dipole tilt as function of time. Bottom: black line shows the relative contribution D of the dipole to the surface magnetic field and the grey line shows the relative contribution $D_{\rm ax}$ of the axial dipole to the surface field. Vertical lines mark the time window for which the VGPs of panel (b) have been calculated. (b) VGP density during the reversal. Black dots give the positions of the true geomagnetic poles.

Tests with 2, 20, 200 and 2000 sites in different distributions (random or regular grid) indicate that with 200 sites in a random distribution we are able to reliably recover the mean distribution of the VGPs. However, variations in the VGP density can clearly be detected with a much smaller number of sites.

3.2.1 VGPs for individual reversals

We start by calculating the VGP distribution for some individual reversals in our Y_{22}-model from Fig. 2. Here we show the fourth, fifth and sixth reversal that occur at times $t_4 = 2.7$, $t_5 = 4.2$ and $t_6 = 4.7$. Blow-ups of the time-series of the dipole tilt centred around the time of reversal are shown in the upper part of panel (a) of the Figs 5, 6 and 7. The lower part of panel (a) shows the relative contribution of the dipole to the surface magnetic field as a function of time. It has been calculated using eq. (5) to determine the energy $W(\ell)$ in the modes $\ell = 1 \ldots 8$. Shown is the relative contribution D of the dipole part to the surface field expanded up to degree and order 8 (at the surface there is little energy in higher modes):

$$D = \sqrt{\frac{W(\ell = 1)}{\sum_{\ell=1}^{8} W(\ell)}}. \qquad (6)$$

For the dipole-dominated field of the present-day Earth $D = 0.97$. In times of stable polarity in our model values of D are typically around 0.95. The relative contribution of the axial dipole $D_{\rm ax}$ to the surface field is obtained using only the g_0^1 term instead of $W(\ell = 1)$ in eq. (6). During a reversal $D_{\rm ax}$ has to vanish at least at some point in time. A large difference between D and $D_{\rm ax}$ indicates the presence of a significant equatorial dipole contribution.

The strong directional change of the dipole takes approximately 0.06 diffusion times (7500 yr) for the reversal in Fig. 5. The density of VGPs taken at 2000 randomly distributed sites during this time interval is shown in Fig. 5(b). The VGPs have been sorted into $10^\circ \times 10^\circ$ bins and their density is normalized by the maximum value. Most VGPs concentrate between longitudes of $\phi = 90^\circ$ and $\phi = 270^\circ$ with a broad maximum at $\phi = 180^\circ$, which is one of the longitudes of maximum CMB heat flux. The connected black dots show the path of the true geomagnetic pole (TGP), i.e. the south pole of the dipole field part alone. It is impossible to determine the site-independent TGP from palaeomagnetic data since the dipole field cannot be separated from the contribution of higher multipoles. For this event the VGPs assemble around the track of the TGP, in agreement with a significant dipole contribution $D > 0.6$ to the transitional field at most times. The difference between $D_{\rm ax}$ (grey

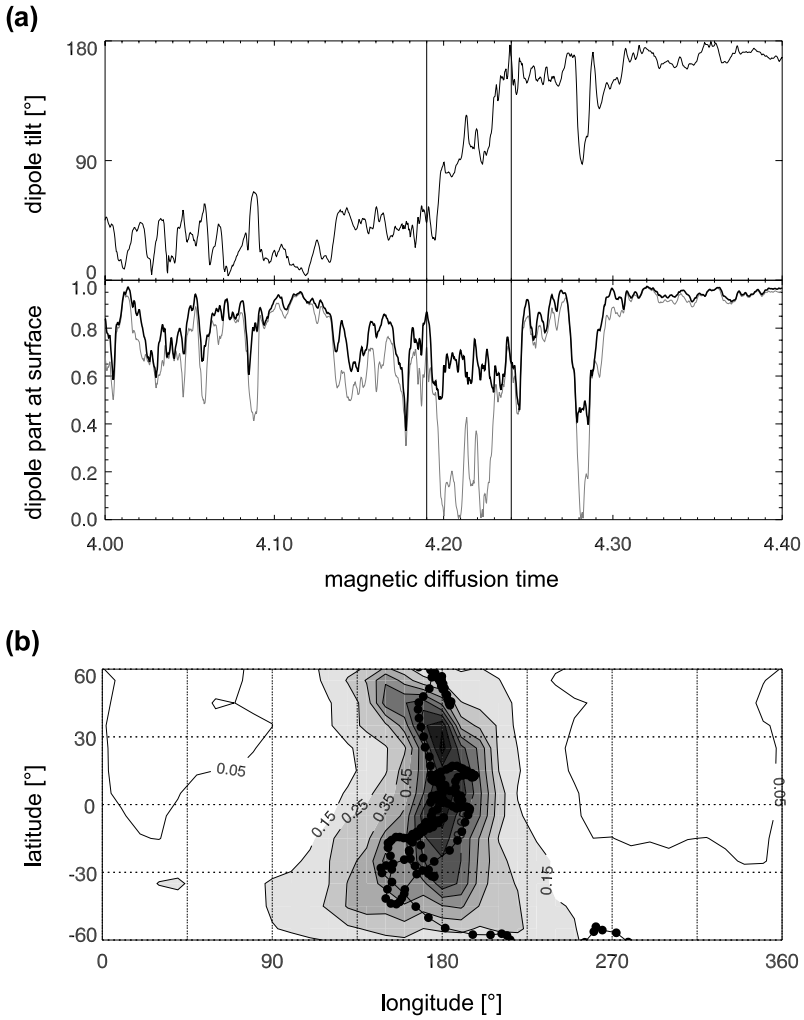

Figure 6. Fifth reversal of the Y_{22} case from Fig. 2. Same representation as in Fig. 5.

line) and D in Fig. 5(a) at times around $t = 2.72$ indicates a strong contribution of the equatorial dipole to the transitional field at the surface.

The fifth reversal (Fig. 6) exhibits a much stronger clustering of the VGPs in a narrow band around $\phi = 180^\circ$. The difference between the total dipole contribution $D \approx 0.65$ and the axial dipole $D_{\rm ax} \approx 0.20$ is large during the transition which takes about 6000 yr (Fig. 6a). Because of the dominance of the equatorial dipole the number of VGPs at $\phi = 180^\circ$ is approximately 10 times larger than the number of VGPs around $\phi = 0^\circ$. The reversal is soon followed by an excursion at $t \approx 4.28$, during which the dipole contribution remains significant. For the excursion the VGPs cluster in a longitude interval between $\phi = 90^\circ$ and $\phi = 135^\circ$ (not shown).

The sixth reversal (Fig. 7) takes about 0.2 diffusion times (25 000 yr), much longer than in the previous cases. There is a long time span where the dipole direction fluctuates and the contribution of the dipole to the surface field is highly variable, with D between 0.3 and 0.8 for most of the time. The resulting VGP density shows maxima at $\phi = 200^\circ$ and around $\phi = 315^\circ$, and a pronounced minimum at $\phi = 90^\circ$. This VGP density function resembles the one deduced by Hoffman (2000) for the Matuyama–Brunhes reversal (see Fig. 3 in his paper) in two aspects. First, it exhibits two longitudes with enhanced VGP density that crudely correlate with the regions of higher than average CMB heat flux in our model. Second, even during the reversal most of the VGPs reside in high latitudes. In the model VGP clusters in different regions are formed at different times during the reversal.

These examples show that the VGP density distribution can differ strongly between reversal events, depending on the contribution of the dipole part to the surface field and the duration of the reversal. One extreme is the strong clustering as in Fig. 6, another the diffuse distribution of VGPs in Fig. 7. Most of the events exhibit VGP distributions somewhere in between, with a preference for the high VGP density to correlate with a longitude of enhanced CMB heat flux. However, there are also examples for events where VGP density and heat flux are uncorrelated.

For the detection of VGP clustering it is not necessary to have as many sites as we used. We have chosen the high number of 2000 sites so that the resulting VGP density is independent of the site distribution. However, tests have shown that the main characteristics of the VGP density are resolved with only five random sites.

3.2.2 Average VGP distribution, Y_{22} pattern

In this section we calculate the long-term average distribution of transitional VGPs, i.e. those which fall within $\pm 60^\circ$ of latitude at any time of the model run (except the first time unit) and at any site. We have used 200 randomly distributed sites. Again we find

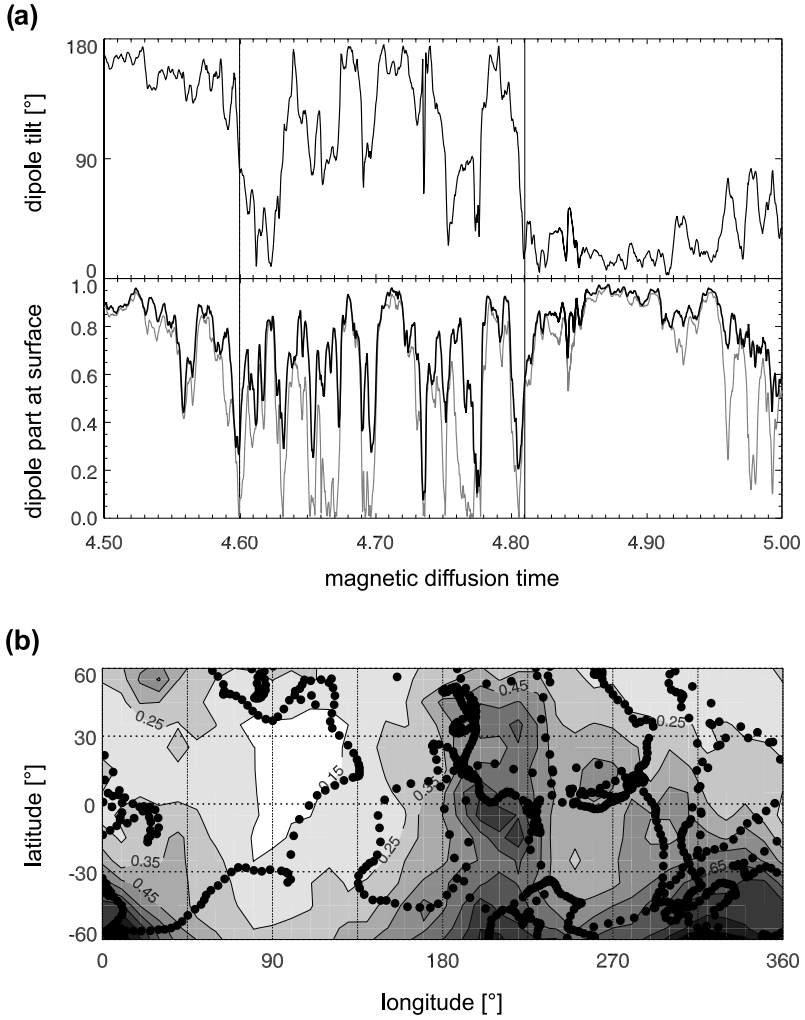

Figure 7. Sixth reversal of the Y_{22} case from Fig. 2. Same representation as in Fig. 5.

that a much smaller number of sites is sufficient to recover the observed clustering. In a test we varied the length of the averaging time interval. The longitudinal variation of the VGP distribution is reasonably well recovered for an averaging time of two or more diffusion times in our model. Because here we average over more than 10 time units we expect the results to be statistically robust.

Fig. 8 shows the mean VGP density of the Y_{22} case at $Ra = 9000$, $f_o = 0.106$ in comparison with that of the homogeneous case. Fig. 8(a) shows the probability for a transitional VGP to fall within a 10° longitude bin. In the homogeneous case the curve approaches a uniform value of $P = 10/360 \approx 2.8$ per cent if averaged over sufficiently long time. For the Y_{22} case there are two peaks in the probability distribution at the maxima of CMB heat flux and two lows at the minima of CMB heat flux. The probability for a VGP to fall within the 0° and 180° bins is about 60 per cent higher than to fall within the 90° and 270° bins. In the homogeneous case the VGP density varies primarily with latitude (Fig. 8b). The small residual longitudinal dependence can be expected to vanish for longer run times of the model. In the examined time interval both models spent more time in normal than in inverse polarity, so that the VGP densities are higher in the Northern Hemisphere. This effect is also expected to vanish in the long run, since for reasons of principle no polarity is preferred over the other. Fig. 8(c) shows the VGP density for the case with the imposed Y_{22} heat flux pattern. Most of the transitional VGPs are found at latitudes larger than ±40° and in equatorial regions the VGP density is low. However, the equatorial VGP density above regions of high CMB heat flux is twice as large as the density above regions of low CMB heat flux.

The CMB heat flux heterogeneity is also reflected in the VGP distributions during time periods of stable polarity. Taking only the VGPs from the time period $t = 6.5$ until $t = 8.5$ with no reversals and two brief events with the dipole axis crossing the equator (compare Fig. 2) gives a similar distribution to the one in Fig. 8(c), only without VGPs in the Southern Hemisphere.

To check the influence of the amplitude of the heat flux heterogeneity we compare the Y_{22} case at $Ra = 9000$ at the amplitudes $f_o = 0.106$ and $f_o = 0.176$. The amplitude of the longitudinal variation of the VGP density increases by a factor of 1.5 in case of the higher heat flow heterogeneity.

In principle, individual VGP reversal paths may depend heavily on the recording site. Gubbins & Sarson (1994) and Gubbins & Love (1998) pointed out that whether a site records the East Asian or the American VGP path depends on the quadrant in which the site is located. Obviously a weak dipole contribution to the transitional field will lead to a strong site dependence of the VGP paths. Depending on the nature of the non-dipole field, the distribution of VGPs recorded at different sites may be rather scattered or could

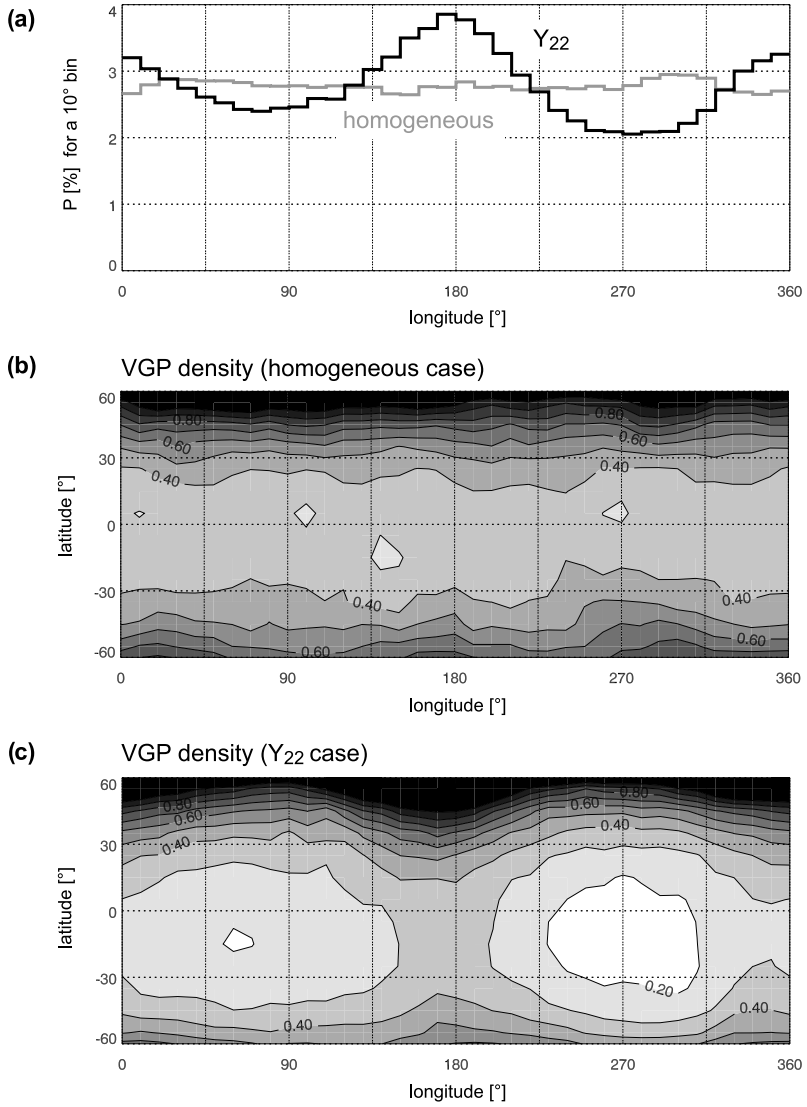

Figure 8. (a) Probability P for a transitional VGP to fall in a 10° longitude bin for the homogeneous case (grey) and the Y_{22} heat flux pattern, $f_o = 0.106$, at $Ra = 9000$ (black). (b) Relative number of VGPs per 10° × 10° interval for the homogeneous case, averaged over five magnetic diffusion times. (c) Same for the Y_{22} case, averaged over 10 magnetic diffusion times. The heat flux maxima are at 0° and 180° longitude.

be more systematic, as in the kinematic dynamo model of Gubbins & Sarson (1994). The relatively strong dipole contribution found during the reversals discussed in the previous section suggests that the clustering of VGPs is due to the dipole part of the field and that the non-dipole field may add a random scatter rather than a systematic contribution to it. We test this by confining the site locations in one case to longitudes of higher than average CMB heat flux ($\phi \in [-45^\circ \ldots 45^\circ] \cup [135^\circ \ldots 225^\circ]$) and in another case to longitudes of lower than average CMB heat flux. For 100 randomly chosen sites in each area and for an averaging time of 8.2 magnetic diffusion times the longitudinal variation of the VGP density is nearly identical in both cases compared with the result for a global distribution of sites. If we further confine the sites in the high heat flow region (or the low heat flow region) to the Northern or Southern Hemisphere, the result is the same. Hence, for our model there is no systematic dependence of the VGP distribution on the area from which the sites are chosen.

3.2.3 Average VGP distribution, tomographic pattern

We now consider the mean VGP densities that arise from the tomographic heat flux pattern (Fig. 1). Because the Y_{22} harmonic makes the largest contribution to the heat flux variation we expect the results to be similar to this case. We chose the amplitude of the dominating Y_{22} mode as $f_o(2, 2) = 0.176$ in one case and half of that value in another case and scaled the amplitudes of the other contributing modes respectively.

Fig. 9 compares the surface energy spectra of the two tomographic models that differ in their amplitude of flux variation. The spectra have been time averaged over 6.5 diffusion times for the model with $f_o(2, 2) = 0.176$ and 3.4 diffusion times for the case with $f_o(2, 2) = 0.088$. The surface fields in both cases are dipole dominated on time average, even though the mean dipole contribution is less than in the Y_{22} case. The model with a high amplitude of heat flux variation has a weaker field and a lower relative contribution of

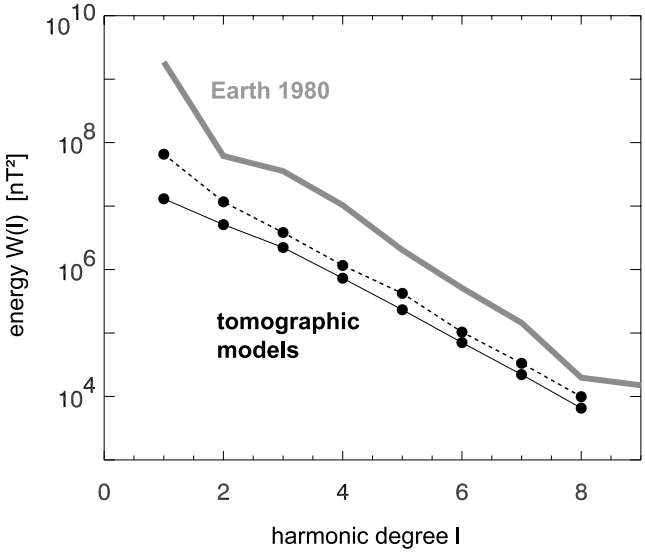

Figure 9. Surface energy spectra of the tomographic models with $f_o(2, 2) = 0.088$ (dashed) and $f_o(2, 2) = 0.176$ (solid). Grey: surface spectrum of the Earth's magnetic field in 1980.

the dipole. On time average, the dipole contributes 15 per cent to the rms field at the CMB for the low-amplitude case, but only 9 per cent in the case of high amplitude. The most frequent value for the tilt of the dipole axis against the rotation axis is about 30° for the high-amplitude model, and about 15° for the low-amplitude model.

The VGP density of the tomographic model at $Ra = 9000$ is given in Figs 10(a) and (b). The model exhibits distinct maxima at geographical longitudes of −100°E and +80°E, that is, the VGPs in the tomographic model prefer the American and East Asian longitudes. Also the actual dipole (TGP) prefers longitudes of high heat flux in the transitional state (Fig. 10c). The maxima in the longitudinal distribution of TGPs with latitudes between −60° and +60° correlate nicely with the longitudes of maximum heat flux in the tomographic case. Moreover, the TGP distribution closely resembles the VGP distribution (Fig. 10a).

We find no big difference in the longitudinal distribution between the tomographic models with different amplitudes of heat flux variation. In the case of the lower amplitude, however, the VGPs tend to lie at higher latitudes so that the VGP density in equatorial regions is less than in the high-amplitude case.

Depending upon the processing and the number and type of data (sedimentary or lava), palaeomagnetic studies have arrived at somewhat different values for the preferred longitudes, e.g. −60°E and +120°E (Laj *et al.* 1992), −80°E and +70°E (Constable 1992) and −105°E and +105°E (Love 1998). The geographical distribution of the Matuyama–Brunhes reversal shows maxima at longitudes of approximately −70°E and +100°E (Clement 1991), that is roughly 25°E of the maxima of our tomographic model. However, in our model the mean VGP distribution does not necessarily reflect the location of clusters in any individual reversal. For the Matuyama–Brunhes reversal there are about four times as many VGPs in the preferred longitudinal bands as in regions of minimal VGP density. For the mean distribution of the tomographic model this factor is only about 1.6, but it can get much larger for individual events.

Olson & Christensen (2002) studied a thermally driven dynamo subject to a CMB heat flux variation of the same geometry as the one used in this study. They found flux concentrations in the time-averaged magnetic field that are displaced slightly to the west compared with the flux patches of the historic geomagnetic field (Bloxham & Jackson 1992). Olson & Christensen (2002) showed that the concentrations in the time-averaged model field move eastwards if more realistic values of the Ekman number are adopted. If this is also true for our model, then the regions of enhanced VGP density are also expected to move eastwards.

4 CAUSE OF VGP CONCENTRATIONS

A longitudinal variation of the heat flux at the CMB leads to an enhanced VGP density above the longitudes of high heat flux. In order to understand the mechanism for the clustering, we analyse the statistical distribution of structures in the velocity field and the magnetic field near the outer boundary. Fig. 11(b) shows the mean of the unsigned (absolute) radial velocity $|v_r|$ slightly below the CMB. As expected, up- and downwelling flow in equatorial regions takes place preferentially at longitudes of enhanced heat flux, whereas there is weak convection in regions of low heat flux, where the top of the core is stably stratified. Radially outward motions of the fluid expel toroidal field from the core, whilst radially inward motions collect the poloidal field by advection. Both effects lead to concentration of magnetic flux in the time-averaged CMB field, which is shown in Fig. 11(a). We find flux concentrations in regions of high heat flow both at high latitudes around ±60° and also within ±20° of the equator.

The origin of these flux concentrations is somewhat different. At high latitudes they are usually of one sign during periods of stable polarity and they are caused by advective accumulation of magnetic flux by downwellings in the time-averaged flow field (Olson & Christensen 2002). At low latitudes, the magnetic flux can have either sign. It seems to originate from flux expulsion and is associated with either upwelling or downwelling flow.

We have seen that the clustering of transitional VGPs is due to the significant equatorial dipole contribution during a reversal. Usually in each longitudinal hemisphere several flux concentrations with different sign are present at the CMB at low latitudes and they cancel to some extent in their contribution to the field at the Earth's surface. However, random fluctuations may lead to an excess of flux of one sign in one hemisphere and of the other sign in the opposite hemisphere and will provide an equatorial dipole contribution to the field. Due to the fact that the magnetic flux tends to concentrate at longitudes of high heat flux, the orientation of the equatorial dipole component will be biased to align with the axis connecting one region of high heat flow to the antipodal one. Even in times where the axial dipole dominates the field, the total dipole will be preferentially tilted along meridians of enhanced heat flux, since the equatorial dipole prefers these longitudes. Therefore the preferred longitudes of higher VGP density appear even in times of stable polarity.

5 CONCLUSIONS

In our numerical dynamo model we find that a non-zonal variation of the heat flux at the CMB results in a longitudinal preference of the transitional VGPs. In the case of a simple heat flux variation according to a Y_{22} harmonic, the VGPs cluster above regions where the heat flux is high. Although the dipole component is weakened in the transitional field, the equatorial dipole remains sufficiently strong and aligns preferentially with regions of high heat flow. Therefore similar VGP distributions are found independent of the recording site. On average the radial movements of the fluid at the top of the

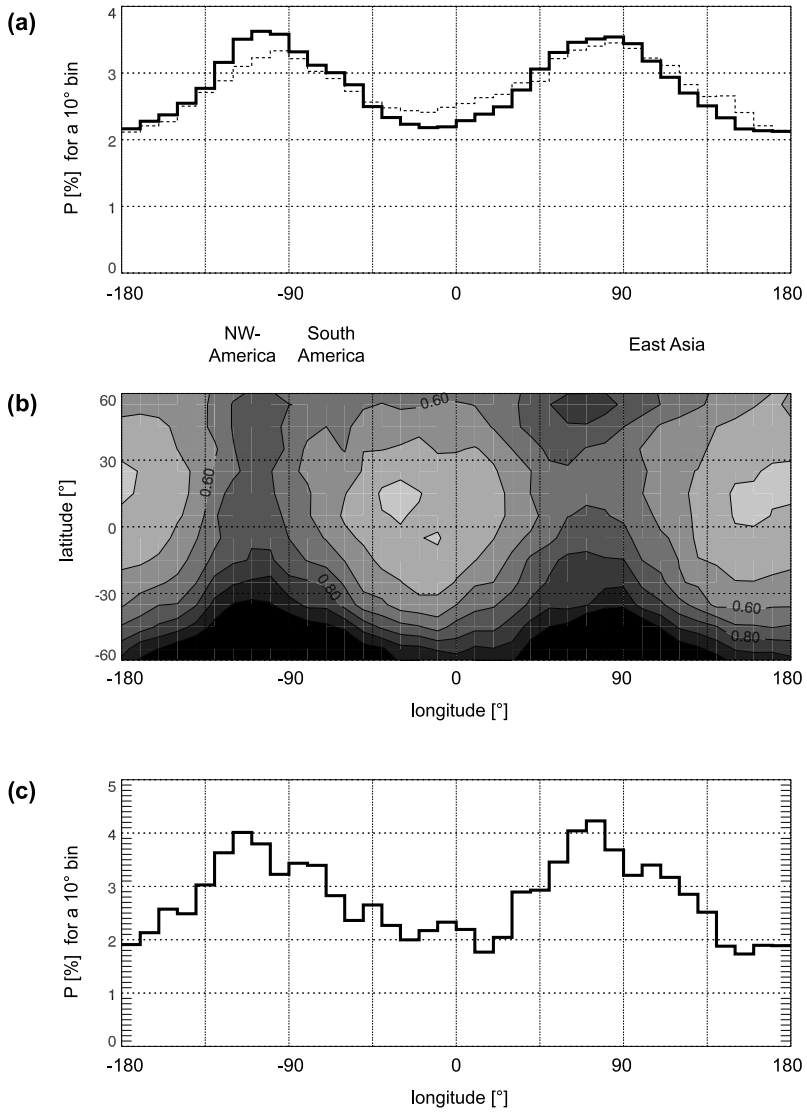

Figure 10. Tomographic case at $Ra = 9000$, $f_o(2, 2) = 0.176$, averaged over 6.5 diffusion times. (a) and (b) The VGP distribution for 200 random sites. (a) Solid line: probability P for a transitional VGP to fall in a 10° longitude bin. (Dashed line shows P for $f_o(2, 2) = 0.088$, averaged over 3.4 diffusion times.) (b) Relative number of VGPs per 10° × 10° interval for $f_o(2, 2) = 0.176$. (c) Distribution of the transitional TGPs with longitude for $f_o(2, 2) = 0.176$.

core are stronger below regions of high heat flux compared with regions of low heat flux. Therefore the average CMB magnetic field strength, and with it the dipole field strength, is higher in longitudes of enlarged heat flux.

Also the VGPs of individual reversals show a preference to fall along one of the two longitudinal bands of enhanced heat flux. However, depending on the reversal length and on how much the dipole contributes to the surface field, the VGP distribution can differ substantially between reversals.

Models with different simple zonal and non-zonal patterns confirm the result by Glatzmaier *et al.* (1999) that the distribution of heat flow at the CMB influences the frequency of reversals. In contrast to that study, which suggest that the amplitude of the heat flux in polar regions is the controlling factor, in our dynamos the the equatorial flux is more important. High equatorial heat flux enhances the reversal frequency whereas low heat flow can suppress reversals entirely.

Our tomographic models show a higher density of the transitional VGPs along American (−100°E) and East Asian (+80°E) longitudes. This is generally consistent with the preferred VGP longitudes found in several palaeomagnetic studies, but shifted slightly towards the west. Our model results therefore support the assumption that the longitudinal bias of the Earth's transitional magnetic field, inferred from some palaeomagnetic studies but disputed by others, is indeed real. Furthermore, they demonstrate that thermal core–mantle coupling is a very plausible cause for the preferred VGP path longitudes.

An interesting implication concerns the nature of seismic velocity anomalies in the deep mantle. It is plausible that both compositional and thermal differences contribute. In particular for the lowermost mantle the observation that the lateral variations in bulk sound speed and shear velocity are anticorrelated (Masters *et al.* 2000, for example) has been taken as evidence that here compositional differences are the primary cause for the velocity anomalies. However, our tomographic heat flow model is based on a purely thermal interpretation of seismic shear wave anomalies in the D″ layer. Its success in reproducing the preferred VGP longitudes suggests that the *S*-wave anomalies mainly reflect the thermal structure in D″ or, perhaps,

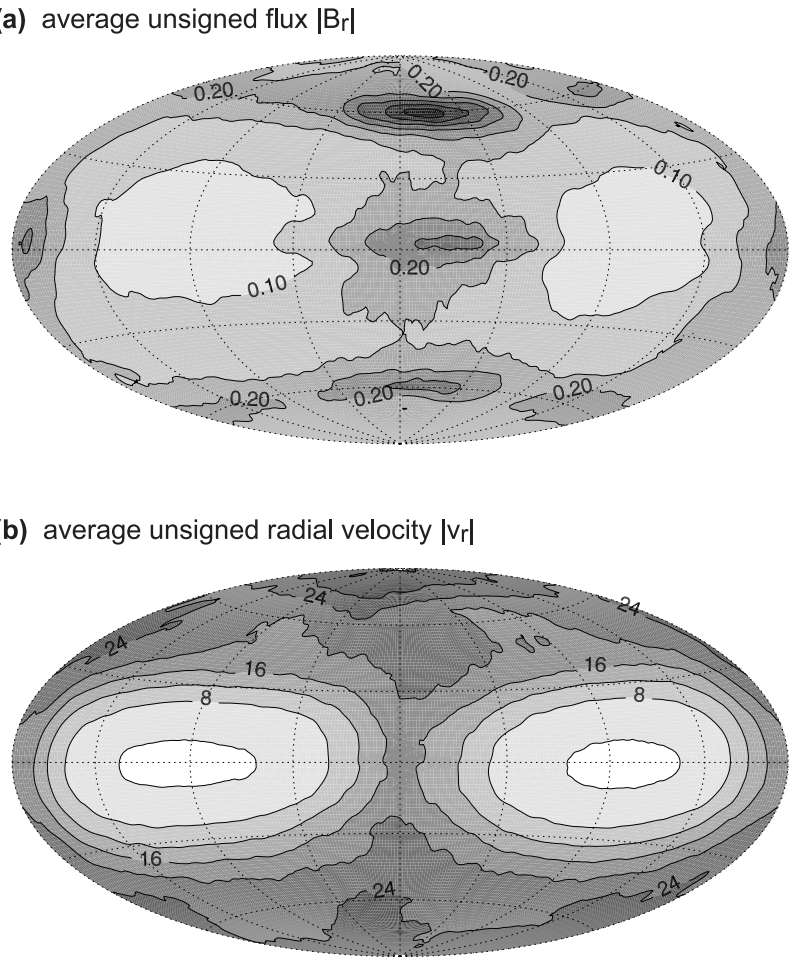

Figure 11. 200 000 yr (1.7 diffusion times) average of $|B_r|$ at the CMB (a) and $|v_r|$ at $0.96r_o$ (b) for the Y_{22} case, $f_o = 0.106$, $Ra = 9000$ in the Aitoff projection. The heat flux maxima are in the middle and at the edge of each figure.

that the compositional anomalies that affect the shear velocity are closely correlated with temperature.

ACKNOWLEDGMENTS

This project is part of the Priority Programme *Geomagnetic Variations* of the Deutsche Forschungsgemeinschaft. We are grateful for support through grant Ch77/11.

REFERENCES

Barton, C.E. & McFadden, P.L., 1996. Inclination shallowing and preferred transitional {VGP} paths, *Earth planet. Sci. Lett.,* **140,** 147–157.

Bloxham, J., 2000. Sensitivity of the geomagnetic axial dipole to thermal core–mantle interactions, *Nature,* **405,** 63–65.

Bloxham, J., 2002. Time-independent and time-dependent behaviour of high-latitude flux bundles at the core–mantle boundary, *Geophys. Res. Lett.,* **29,** 1854, doi:10.1029/2001GL014543.

Bloxham, J. & Gubbins, D., 1987. Thermal core–mantle interactions, *Nature,* **325,** 511–513.

Bloxham, J. & Jackson, A., 1992. Time-dependent mapping of the magnetic field at the core–mantle boundary, *J. geophys. Res.,* **97,** 19 537–19 563.

Braginsky, S.I. & Roberts, P.H., 1995. Equations governing convection in earth's core and the geodynamo, *Geophys. Astrophys. Fluid Dyn.,* **79,** 1–97.

Brito, D., Arnou, J. & Olson, P., 1999. Can heterogeneous electromagnetic coupling control geomagnetic reversals, *Phys. Earth planet. Int.,* **112,** 159–170.

Brunhes, B., 1906. Récherches sur le directions d'aimantation des roches volcaniques, *J. Physique,* **5,** 705–724.

Christensen, U.R. & Olson, P., 2003. Secular variation in numerical geodynamo models with lateral variations of boundary heat flow, *Phys. Earth planet. Int.,* **138,** 39–54.

Christensen, U.R., Olson, P. & Glatzmaier, G.A., 1999. Numerical modelling of the geodynamo: a systematic parameter study, *Geophys. J. Int.,* **138,** 393–409.

Clement, B.M., 1991. Geographical distribution of transitional VGPs: evidence for non-zonal equatorial symmetry during the Matuyama–Brunhes geomagnetic reversal, *Earth planet. Sci. Lett.,* **104,** 48–58.

Clement, B.M. & Kent, D.V., 1991. A southern hemisphere record of the Matuyama–Brunhes polarity reversal, *Geophys. Res. Lett.,* **18,** 81–84.

Coe, R.S., Hongre, L. & Glatzmaier, G.A., 2000. An examination of simulated geomagnetic reversals from a palaeomagnetic perspective, *Phil. Trans. R. Soc. Lond.,* A, **358,** 1141–1170.

Constable, C.G., 1992. Link between geomagnetic reversal paths and secular variation of the field over the past 5 My, *Nature,* **358,** 230–233.

Creer, K.M. & Ispir, Y., 1970. An interpretation of the behaviour of the geomagnetic field during polarity transitions, *Phys. Earth planet. Int.,* **2,** 283–293.

Dormy, E., Valet, J.-P. & Courtillot, V., 2000. Numerical models of the geodynamo and observational constraints, *Geochem. Geophys. Geosyst.,* **1,** article no 2000GC000062.

Dziewonski, A.M. & Woodhouse, J.H., 1987. Global images of the Earth's interior, *Science,* **236,** 37–48.

Gibbons, S.J. & Gubbins, D., 2000. Convection in the Earth's core driven by lateral variations in the core-mantle boundary heat flux, *Geophys. J. Int.,* **142,** 631–642.

Glatzmaier, G.A., 1984. Numerical simulations of stellar convective dynamos. I. The model and method, *J. Comput. Phys.,* **55,** 461–484.

Glatzmaier, G.A. & Roberts, P.H., 1997. Simulating the geodynamo, *Contemp. Phys.,* **38,** 269–288.

Glatzmaier, G.A., Coe, R.S., Hongre, L. & Roberts, P.H., 1999. The role of the Earth's mantle in controlling the frequency of geomagnetic reversals, *Nature,* **401,** 885–890.

Gubbins, D. & Love, J.J., 1998. Preferred VGP paths during geomagnetic polarity reversals: symmetry considerations, *Geophys. Res. Lett.,* **25**(7), 1079–1082.

Gubbins, D. & Sarson, G., 1994. Geomagnetic field morphologies from a kinematic dynamo model, *Nature,* **368,** 51–55.

Hide, R., 1967. Motions of the Earth's core and mantle, and variations of the main geomagnetic field, *Science,* **157,** 55–56.

Hillhouse, J. & Cox, A., 1976. Brunhes–Matuyama polarity transition, *Earth planet. Sci. Lett.,* **29,** 51–64.

Hoffman, K.A., 2000. Temporal aspects of the last reversal of the Earth's magnetic field, *Phil. Trans. R. Soc. Lond.,* A, **358,** 1181–1190.

Jackson, A., Jonkers, A.R.T. & Walker, M.R., 2000. Four centuries of geomagnetic secular variation from historical records, *Phil. Trans. R. Soc. Lond.,* A, **358,** 957–990.

Kutzner, C. & Christensen, U.R., 2002. From stable dipolar towards reversing numerical dynamos, *Phys. Earth planet. Int.,* **131,** 29–45.

Laj, C., Mazaud, A., Weeks, R., Fuller, M. & Herrero-Bervera, E., 1991. Geomagnetic reversal paths, *Nature,* **351,** 447.

Laj, C., Mazaud, A., Weeks, R., Fuller, M. & Herrero-Bervera, E., 1992. Statistical assessment of the preferred longitudinal bands for recent geomagnetic reversal records, *Geophys. Res. Lett.,* **19,** 2003–2006.

Langel, R.A. & Estes, R.H., 1982. A geomagnetic field spectrum, *Geophys. Res. Lett.,* **9,** 250–253.

Langereis, C.G., Hoof, A.A.M.V. & Rochette, P., 1992. Longitudinal confinement of geomagnetic reversal paths as a possible sedimentary artefact, *Nature,* **358,** 226–230.

Love, J.J., 1998. Paleomagnetic volcanic data and geometric regularity of reversals and excursions, *J. Geophys. Res.,* **103,** 12 435–12 452.

Love, J.J., 2000. Statistical assessment of preferred transitional VGP longitudes based on paleomagnetic lava data, *Geophys. J. Int.,* **140,** 211–221.

Masters, G., Johnson, S., Laske, G. & Bolton, H., 1996. A shear-velocity model of the mantle, *Phil. Trans. R. Soc. Lond.,* A, **354,** 1385–1411.

Masters, G., Laske, G., Bolton, H. & Dziewonski, A., 2000. The relative behavior of shear velocity, bulk sound speed, and compressional velocity in the mantle: implications for chemical and thermal structure, in *Earth's Deep Interior: Mineral Physics and Tomography from the Atomic to the Global Scale,* American geophysical Union Geophysical Monograph 117, pp. 63–87, eds Karato, S.-I., Forte, A.M., Liebermann, R.C., Masters, G. & Stixrude, L., American Geophysical Union, Washington, DC.

Merrill, R.T. & McFadden, P.L., 1999. Geomagnetic polarity transitions, *Rev. Geophys.,* **37,** 201–226.

Niitsuma, N., 1971. Paleomagnetic and paleoenvironmental study of sediments recording Matuyama–Brunhes geomagnetic reversal, *Tohoku Univ. Sci. Rep., Geol.,* **43,** 1–39.

Olson, P. & Christensen, U.R., 2002. The time-averaged magnetic field in numerical dynamos with non-uniform boundary heat flow, *Geophys. J. Int.,* **151,** 809–823.

Olson, P., Christensen, U.R. & Glatzmaier, G.A., 1999. Numerical modeling of the geodynamo: mechanisms of field generation and equilibration, *J. geophys. Res.,* **104,** 10 383–10 404.

Prévot, M. & Camps, P., 1993. Absence of preferred longitude sectors for poles from volcanic records of geomagnetic reversals, *Nature,* **366,** 53–57.

Runcorn, S.K., 1992. Polar path in geomagnetic reversals, *Nature,* **356,** 654–656.

Sarson, G.R., Jones, C.A. & Longbottom, A.W., 1997. The influence of boundary layer heterogeneities on the geodynamo, *Phys. Earth planet. Int.,* **101,** 13–32.

Secco, R.A. & Schloessin, H.H., 1989. The electrical resistivity of solid and liquid Fe at pressures up to 7 GPa, *J. geophys. Res.,* **94,** 5887–5894.

Selkin, P.A. & Tauxe, L., 2000. Long-term variations in paleointensity, *Phil. Trans. R. Soc. Lond.,* A, **358,** 1065–1088.

Steinhauser, P. & Vincenz, S.A., 1973. Equatorial paleopoles and behaviour of the dipole field during polarity transitions, *Earth planet. Sci. Lett.,* **19,** 113–119.

Tric, E., Laj, C., Jéhanno, C., Valet, J.-P., Kissel, C., Mazaud, A. & Iaccarino, S., 1991. High-resolution record of the Upper Olduvai transition from Po Valley (Italy) sediments: support for dipolar transition geometry?, *Phys. Earth planet. Int.,* **65,** 319–336.

Valet, J.P., Tucholka, P., Courtillot, V. & Meynadier, L., 1992. Paleomagnetic constraints on the geometry of the geomagnetic field during reversals, *Nature,* **356,** 400–407.

van Zijl, J.S.V., Graham, W.T. & Hales, A.L., 1962. The palaeomagnetism of the Stormberg Lavas, II. The behaviour of the magnetic field during a reversal, *Geophys. J. R. astron. Soc.,* **7,** 169–182.

Wicht, J., 2002. Inner-core conductivity in numerical dynamo simulations, *Phys. Earth planet. Int.,* **132,** 281–302.